IOSR Journal of Mathematics (IOSR-JM)
e-ISSN: 2278-0661, p-ISSN: 2278-8727, Volume 21, Issue 2, Ser. 3 (Mar. – Apr. 2025), PP 01-11
www.iosrjournals.org

Thermal Applications Of Carbon Nanotubes In Polyethylene Glycol In The Presence Of Magnetic Field On Electronic Devices

Winfred Muteti, Isaac Chepkwony
(Mathematics And Actuarial Science, Kenyatta University, Kenya)
(Mathematics And Actuarial Science, Kenyatta University, Kenya)

Abstract:
Background*: In this study, the thermal management of electronic devices, specifically CPUs, using carbon nanotubes (CNT) dispersed in polyethylene glycol (PEG-400) under the influence of a magnetic field was studied. The research aims to optimize cooling performance by enhancing efficiency, extending the operating temperature range, and improving the reliability of such systems.*
Materials and Methods*: The study modeled impingement cooling using a Darcy-Brinkman-Forchheimer approach and considered the effects of viscous dissipation. The governing nonlinear partial differential equations were converted into nonlinear ordinary differential equations (ODEs) by utilizing similarity variables and solved using numerical methods. CNT-PEG-400 nanofluid flowing via a porous metal foam CPU cooler with a fan and a heated CPU surface was simulated.*
Results*: The investigation of key parameters like Hartmann number, Reynolds number, Darcy number, and porosity revealed that increasing the Darcy number significantly enhances heat transfer. The Hartmann number's effect varies with porosity, where stronger magnetic fields are advantageous for highly porous metal foams, ultimately improving cooling efficiency.*
Conclusion: *CNTs increase both the density and viscosity of PEG-400, leading to enhanced heat transfer characteristics, which improve overall cooling performance. These findings contribute to optimizing cooling strategies for CPUs and other electronic devices, especially when using CNT-PEG-400 nanofluids in the presence of magnetic fields.*
Key Word*: Hartmann Number; Nusselt Number; Porosity; Heat Transfer; Viscosity; Density; Thermal Conductivity; Single-phase Nanofluid*

Date of Submission: 13-04-2025 Date of Acceptance: 23-04-2025

I. Introduction

Electronic devices generate heat during operation, and efficient thermal management is necessary for their optimal performance and longevity. Conventional cooling methods for electronic devices, such as air cooling and liquid cooling, have limitations in terms of efficiency and size, particularly for high-power devices. Due to their exceptional thermal conductivity, carbon nanotubes (CNTs) have become a highly promising material for thermal management applications.

Nanofluids containing carbon nanotubes (CNTs) dispersed in a base fluid such as polyethylene glycol (PEG-400) have demonstrated improved thermal properties. These enhanced fluids show potential for use as coolants in electronic devices. Furthermore, in the presence of a magnetic field, CNT-based nanofluids exhibit unique thermal properties due to CNTs alignment along the magnetic field direction. This alignment results in enhanced thermal conductivity that can bring about improved thermal management of electronic devices (Yu et al., 2021).

Electronic devices that can benefit from this technology include, graphics processing units (GPUs), high-power microprocessors (CPUs), field-programmable gate arrays (FPGAs), and other high-performance computing components. These devices typically operate most efficiently within a specific temperature range. For instance, Central Processing Units typically operate most efficiently within a temperature range of 30°C to 70°C, with a maximum safe operating temperature of around 100°C. GPUs can function at higher temperatures of up to 85°C to 100°C, depending on the specific model and manufacturer.

Effective thermal management techniques, such as CNT-based nanofluids, can help extend the temperature range at which electronic devices can operate efficiently and safely. On this study, we focus on heat dissipation on miniature electronic devices like CPUs so as to maintain their operational efficiency and ensure long-term reliability and performance. Thus, the use of CNT in PEG-400 is a promising approach for thermal management of electronic devices in magnetic field's presence, particularly for high-power devices.

II. Methodology

The current investigation employs a modeling framework based on a CPU cooling system using CNT in PEG-400 nanofluid as in figure 1.

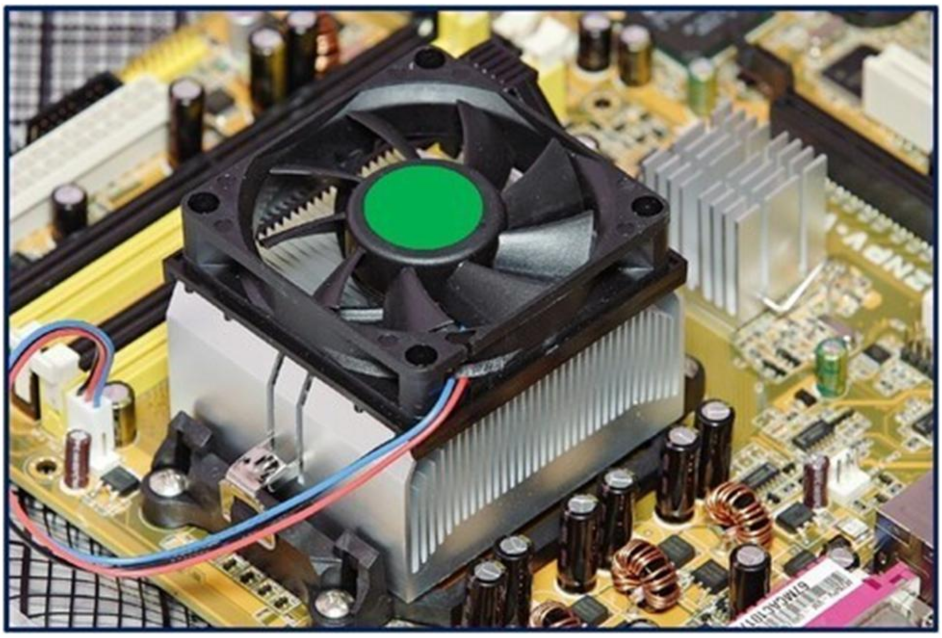

Figure 1 CPU cooling system model

The CPU is modeled as having a metal foam heat sink, which is responsible for dissipating heat. However, the CPU's and heat sink's thermal resistance is neglected. Due to the low Reynolds number, the flow field within the porous media is assumed to be laminar. The physical properties of the CNT-PEG-400 nanofluid are assumed to be constant and not affected by changes in temperature, and a uniform constant magnetic field is applied to the heat sink.

The heat sink's physical properties are assumed to be isotropic and homogeneous with no temperature variability. Due to high flow resistance in the porous medium, I have considered heat generated by both the friction between the CNT-PEG-400 and the solid pores and viscous dissipation.

Assumptions:

- The nanofluid is assumed to be incompressible and steady
- The viscosity of the nanofluid is consistent and unaffected by shear rate.
- Nanofluid's thermal conductivity is uniform in all directions.
- The metal foam maintains consistent porosity, allowing fluid to flow uniformly through the pores in all directions.
- The magnetic field's intensity and orientation are consistent throughout the study area.
- In the investigation of the porous media, both viscous and inertial forces are taken into consideration.
- Heat is uniformly distributed across the CPU's surface, with no heat transfer occurring through the model's side walls.
- At the porous medium's wall, the flow velocity of the nanofluid is zero.

Mathematical formulation of the problem:

The problem is modelled by assuming that in the process of heat dissipation, the drop in pressure and transfer of heat is assumed to be constant, when exposed to a uniformly applied jet velocity. This flow is assumed to be like the flow that occurs between parallel plates. The flow is parallel to the x-axis, with a uniform velocity distribution along the y-axis, while the heat is being generated. The cooling nanofluid exits the fan with a constant velocity, Uin, and temperature, Tin. It subsequently enters the heat sink uniformly. Since the CPU's surface is expected to maintain a fixed temperature, we assume the surface maintains a constant temperature, Tw. A magnetic field which is uniform is applied to the porous medium. As the nanofluid flows through the porous metal foam, it effectively transfers the heat generated by the CPU surface to the heat sink boundary.

Fundamental equations:
Continuity equation:

$$\frac{\partial u}{\partial x}+\frac{\partial v}{\partial y}=0$$

Momentum equation:
x-momentum:

$$\frac{1}{\varepsilon^2}\left(u\frac{\partial u}{\partial x}+v\frac{\partial u}{\partial y}\right)=-\frac{1}{\rho_{nf}}\frac{\partial p}{\partial x}+\frac{\vartheta_{nf}}{\varepsilon}\left(\frac{\partial^2 u}{\partial x^2}+\frac{\partial^2 u}{\partial y^2}\right)-\left(\frac{\sigma_{nf}}{\rho_{nf}}B_0^2+\frac{\vartheta_{nf}}{K^*}+\frac{C_E}{\sqrt{k^*}}\sqrt{u^2+v^2}\right)u$$

y-momentum:

$$\frac{1}{\varepsilon^2}\left(u\frac{\partial v}{\partial x}+v\frac{\partial v}{\partial y}\right)=-\frac{1}{\rho_{nf}}\frac{\partial p}{\partial y}+\frac{\vartheta_{nf}}{\varepsilon}\left(\frac{\partial^2 v}{\partial x^2}+\frac{\partial^2 v}{\partial y^2}\right)-\left(\frac{\sigma_{nf}}{\rho_{nf}}B_0^2+\frac{\vartheta_{nf}}{K^*}+\frac{C_E}{\sqrt{k^*}}\sqrt{u^2+v^2}\right)v$$

Where:
ε is medium's porosity
k^* stands for the thermal conductivity
T represents the temperature
σ_{nf} denotes the electrical conductivity of the nanofluid
K^* signifies the permeability of the porous medium.
ρ_{nf} stands for the density of the nanofluid
$C_E$is the coefficient of form drag
ϑ_{nf} indicates the kinematic viscosity of the nanofluid
B_0 is the magnetic field strength that is applied
σ_{nf} is the electrical conductivity of the nanofluid.
$\frac{\vartheta_{nf}}{K^*}u$ represents the Darcy term.
$\left(\frac{C_E}{\sqrt{k^*}}\sqrt{u^2+v^2}\right)u$ represents the Forchheimer term.

The Lorentz force, resulting from the interaction between the magnetic field and the moving nanofluid, is represented by the term $\frac{\sigma_{nf}}{\rho_{nf}}B_0^2$

$\frac{C_E}{\sqrt{k^*}}$ accounts for the drag force within the porous medium

Energy equation

$$u\frac{\partial T}{\partial x}+v\frac{\partial T}{\partial y}=\frac{k_{eff}}{(\rho C_p)_{nf}}\left(\frac{\partial^2 T}{\partial x^2}+\frac{\partial^2 T}{\partial y^2}\right)+\frac{Q^*}{(\rho C_p)_{nf}}(T-T_{in})+\Phi$$

Where:

$$\Phi=\frac{\mu_{nf}}{K^*}(u^2+v^2)+\frac{\mu_{nf}}{\varepsilon}\left\{2\left(\frac{\partial u}{\partial x}\right)^2+\left(\frac{\partial v}{\partial y}\right)^2+\left(\frac{\partial v}{\partial x}+\frac{\partial u}{\partial y}\right)^2\right\}$$

k_{eff} is the effective thermal conductivity
$(\rho)_{nf}$ is the density for the nanofluid.
The specific heat capacity of the nanofluid is denoted as $(C_p)_{nf}$
Φ represents the viscous dissipation effects.

Boundary Conditions:
Inlet boundary: Located at y = H, where the nanofluid enters the channel:
u = 0, v = $-U_{in}$, T= T_{in}
Wall: Located at y = 0 (no-slip wall):
u = 0 = v, T= T_w

Nanofluid thermophysical properties

Table 1 properties of the nanoparticles and base fluid (Yin et al., 2008, Narang & Pundir, 2018, Marcos et al., 2019)

	$\rho(kg/m^3)$	$C_p(J/Kg.K)$	$k(W/m.K)$	$\sigma(\Omega\text{m})^{-1}$
PEG-400	1125	2400	0.186	10^{-8}
CNTs	1400	700	4000	10^{8}

Table 2 properties of the Metal foam (Calmidi et al., 2000)

	Porosity	c_E	K(x$10^7 m^2$)	$k_s(W/m.K)$
Metal foam	0.9118	0.085	1.8	95

Table 3 reference values

H/L	c_E	ε	X	ϕ	Da_H	Ha_H	Ec_H
1	0.09	0.9	1	0.05	5×10^{-3}	20	0.001

Viscosity
Using Brinkman equation, the viscosity is:

$$\mu_{nf} = 102.31 mPa.s$$

The viscosity of the nanofluid increases slightly in comparison with the viscosity of the base fluid due to the addition of CNTs.

Density
Using the rule of mixtures, the density of the nanofluid is:

$$\rho_{nf} = 1.1616 \text{ g/cm}^3$$

Effective thermal conductivity

$$k_{eff} = \varepsilon k_{nf} + (1-\varepsilon)k_s$$

Where

$$\frac{k_{nf}}{k_{bf}} = \frac{k_{np} + 2k_{bf} - 2\phi(k_{bf} - k_{np})}{k_{np} + 2k_{bf} + \phi(k_{bf} - k_{np})}$$

The effective thermal conductivity of the CNT-PEG-400 nanofluid is calculated to be 0.2154 W/m.K. Consequently, the effective thermal conductivity is determined to be 9.69386 W/m.K.

Normalization of governing equations
To nondimensionalize the above equations, the following dimensionless variables are used:

$$U = \frac{u}{U_{in}}, V = \frac{v}{U_{in}}, P = \frac{p}{\rho_{nf} U_{in}^2}, X = \frac{x}{H}, Y = \frac{y}{H}, \theta = \frac{T - T_{in}}{T_w - T_{in}}$$

The continuity equation becomes:

$$\frac{\partial U}{\partial X} + \frac{\partial V}{\partial Y} = 0 \qquad (1)$$

Doing the same for the momentum equations and using the Darcy number (Da_H), Eckert number (Ec), heat source (Q), Reynolds number (Re_H), Hartmann number (Ha_H), Prandtl number (Pr), convection (λ_H), and distance from the symmetric axis (X), dimensionless parameters expressed as:

$$Da_H = \frac{K}{H^2} = (\frac{L}{H})^2 \frac{K}{L^2} = (\frac{H}{L})^{-2} Da_L, \qquad Ec = \frac{U_{in}^2}{(Cp)_{nf}(T_w - T_{in})}, \qquad Q = \frac{Q^* H^2}{\vartheta_{nf}(\rho Cp)_{nf}},$$

$$Re_H = \frac{HU_{in}}{\vartheta_{nf}} = \left(\frac{H}{L}\right)\frac{LU_{in}}{\vartheta_{nf}} = \left(\frac{H}{L}\right) Re_L, \qquad Ha_H = HB\sqrt{\frac{\sigma_{nf}}{\mu_{nf}}} = \left(\frac{H}{L}\right) LB\sqrt{\frac{\sigma_{nf}}{\mu_{nf}}} = \left(\frac{H}{L}\right) Ha_L,$$

$$Pr = \frac{\vartheta_{nf}(\rho Cp)_{nf}}{k_{nf}}, \qquad \lambda = \frac{Gr}{Re_H}, \qquad X = \frac{x}{H} = \left(\frac{L}{H}\right)\frac{x}{L} = (\frac{H}{L})^{-1} X_L,$$

$$Gr = \frac{g\beta_{nf} H}{U_{in}^2}(T_w - T_{in})$$

we get:

x-momentum:

$$\frac{1}{\varepsilon^2}\left(u\frac{\partial u}{\partial x} + v\frac{\partial u}{\partial y}\right) = -\frac{1}{\rho_{nf}}\frac{\partial p}{\partial x} + \frac{\vartheta_{nf}}{\varepsilon}\left(\frac{\partial^2 u}{\partial x^2} + \frac{\partial^2 u}{\partial y^2}\right) - \left(\frac{\sigma_{nf}}{\rho_{nf}} B_0^2 + \frac{\vartheta_{nf}}{K^*} + \frac{C_E}{\sqrt{k^*}}\sqrt{u^2 + v^2}\right) u$$

y-momentum:

$$\frac{1}{\varepsilon^2}\left(u\frac{\partial v}{\partial x} + v\frac{\partial v}{\partial y}\right) = -\frac{1}{\rho_{nf}}\frac{\partial p}{\partial y} + \frac{\vartheta_{nf}}{\varepsilon}\left(\frac{\partial^2 v}{\partial x^2} + \frac{\partial^2 v}{\partial y^2}\right) - \left(\frac{\vartheta_{nf}}{K^*} + \frac{C_E}{\sqrt{k^*}}\sqrt{u^2 + v^2}\right) v$$

The x-momentum equation becomes:

$$\frac{1}{\varepsilon^2}\left(U\frac{\partial U}{\partial X}+V\frac{\partial U}{\partial Y}\right)=-\frac{\partial P}{\partial X}+\frac{1}{\varepsilon Re_H}\left(\frac{\partial^2 U}{\partial X^2}+\frac{\partial^2 U}{\partial Y^2}\right)-\frac{1}{Re_H Da_H}U-\frac{c_E}{\sqrt{Da_H}}\left(\sqrt{U^2+V^2}\right)U-\frac{Ha_H^2}{Re_H}U \quad (2)$$

And the y-momentum becomes:

$$\frac{1}{\varepsilon^2}\left(U\frac{\partial V}{\partial X}+V\frac{\partial V}{\partial Y}\right)=-\frac{\partial P}{\partial Y}+\frac{1}{\varepsilon Re_H}\left(\frac{\partial^2 V}{\partial X^2}+\frac{\partial^2 V}{\partial Y^2}\right)-\frac{1}{Re_H Da_H}V-\frac{c_E}{\sqrt{Da_H}}\left(\sqrt{U^2+V^2}\right)V \quad (3)$$

The energy equation becomes:

$$PrRe_H\left(U\frac{\partial \theta}{\partial X}+V\frac{\partial \theta}{\partial Y}\right)=\left(\frac{\partial^2 \theta}{\partial X^2}+\frac{\partial^2 \theta}{\partial Y^2}\right)+PrEc\left\{\frac{1}{Da_H}(U^2+V^2)+\frac{1}{\varepsilon}\left(2\left[\left(\frac{\partial U}{\partial X}\right)^2+\left(\frac{\partial V}{\partial Y}\right)^2\right]+\left[\frac{\partial U}{\partial Y}+\frac{\partial V}{\partial X}\right]^2\right)\right\} \quad (4)$$

Similarity Solution

According to the research done by Feng et al., 2015, equations (1) to (3) can be formulated as:

$$\frac{\partial U}{\partial X}+\frac{\partial V}{\partial Y}=0 \quad (5)$$

$$\frac{1}{\varepsilon^2}\left(U\frac{\partial U}{\partial X}+V\frac{\partial U}{\partial Y}\right)=-\frac{\partial P}{\partial X}+\frac{1}{\varepsilon Re_H}\left(\frac{\partial^2 U}{\partial X^2}+\frac{\partial^2 U}{\partial Y^2}\right)-\frac{1}{Re_H Da_H}U-\frac{c_E}{\sqrt{Da_H}}|U|U-\frac{Ha_H^2}{Re_H}U \quad (6)$$

$$\frac{1}{\varepsilon^2}\left(U\frac{\partial V}{\partial X}+V\frac{\partial V}{\partial Y}\right)=-\frac{\partial P}{\partial Y}+\frac{1}{\varepsilon Re_H}\left(\frac{\partial^2 V}{\partial X^2}+\frac{\partial^2 V}{\partial Y^2}\right)-\frac{1}{Re_H Da_H}V-\frac{c_E}{\sqrt{Da_H}}|V|V \quad (7)$$

We can then use the following similarity parameters

$$U=Xf'(Y),\ V=-f(Y),\ \theta=\theta(Y) \quad (8)$$

Substituting the transformations, (6) & (7) become:

$$\frac{\partial P}{\partial X}=X\left(\frac{1}{\varepsilon^2}(ff''-f'^2)+\frac{1}{\varepsilon Re_H}f'''-\frac{1}{Re_H}\left(\frac{1}{Da_H}+Ha_H^2\right)f-\frac{c_E}{\sqrt{Da_H}}Xf'^2\right) \quad (9)$$

$$\frac{\partial P}{\partial Y}=\frac{1}{Re_H Da_H}f+\frac{c_E}{\sqrt{Da_H}}f^2-\frac{1}{\varepsilon Re_H}f''-\frac{1}{\varepsilon^2}ff' \quad (10)$$

Eliminating the pressure gradient, we get a 4th order non-linear ode:

$$f^{iv}+\frac{Re_H}{\varepsilon}ff'''-\left(2c_E\varepsilon X\frac{Re_H}{\sqrt{Da_H}}+\frac{Re_H}{\varepsilon}\right)f'f''-\varepsilon\left(\frac{1}{Da_H}+Ha_H^2\right)f''=0 \quad (11)$$

Considering the following boundary conditions:

$$f(0)=0, f'(0)=0, f(1)=1, f'(1)=0 \quad (12)$$

We are going to let:

$$y_1=f,\qquad y_2=f',\qquad y_3=f'',\qquad y_4=f'''$$

Then the system becomes:

$$y_1'=y_2$$
$$y_2'=y_3$$
$$y_3'=y_4$$
$$y_4'=-\frac{Re_H}{\varepsilon}y_1y_4+\left(2c_E\varepsilon X\frac{Re_H}{\sqrt{Da_H}}+\frac{Re_H}{\varepsilon}\right)y_2y_3+\varepsilon\left(\frac{1}{Da_H}+Ha_H^2\right)y_3$$

The BCs become:

$$y_1(0)=0,\qquad y_2(0)=0,\qquad y_1(1)=1,\qquad y_2(1)=0$$

This has then been solved using MATLAB's bvp4c.

The energy equation can also be transformed to the following, by employing the similarity analysis:

$$\theta''+PrRe_H f\theta'+PrEc\left\{\frac{1}{Da_H}(X^2f'^2+f^2)+\frac{1}{\varepsilon}(4f'^2+X^2f''^2)\right\}=0 \quad (13)$$

With the B.Cs:

$$\theta(0)=1, \theta(1)=0 \quad (14)$$

To transform the energy equation into a system of first-order ordinary differential equations (ODEs), we define:

$$y_1 = \theta, \qquad y_2 = \theta'$$

Then, the system becomes:

$y_1' = y_2$

$$y_2' = -PrRe_H f y_2 - PrEc\left(\frac{1}{Da_H}(X^2 f'^2 + f^2) + \frac{1}{\varepsilon}(4f'^2 + X^2 f''^2)\right)$$

To analyze the heat transfer efficiency of CNT-PEG-400, the Nusselt number will be calculated using the following equations:

$$Nu = \frac{hL}{k_{bf}} \ where: h = \frac{q''_{wall}}{\Delta T} \ and \ q''_{wall} = -k_{eff}(\frac{\partial T}{\partial y}|_{y=0} = -k_{eff}\frac{\Delta T}{H}\theta'(0) \qquad (15)$$

$$=> Nu = -\frac{k_{eff}}{k_{bf}}\left(\frac{H}{L}\right)^{-1}\theta'(0) \qquad (16)$$

III. Result

Darcy number study

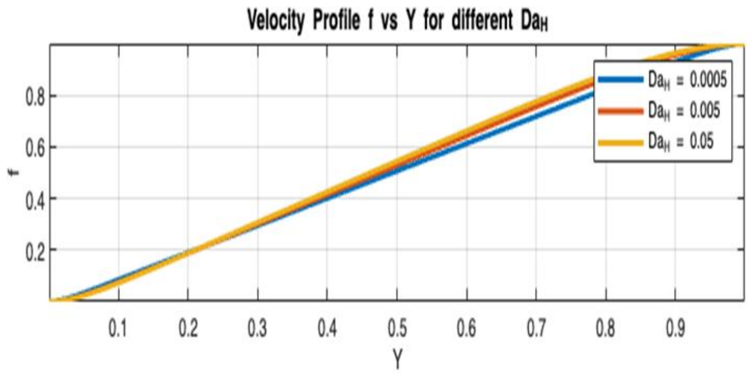

Figure 1 (a) variation of f with respect to Da_H

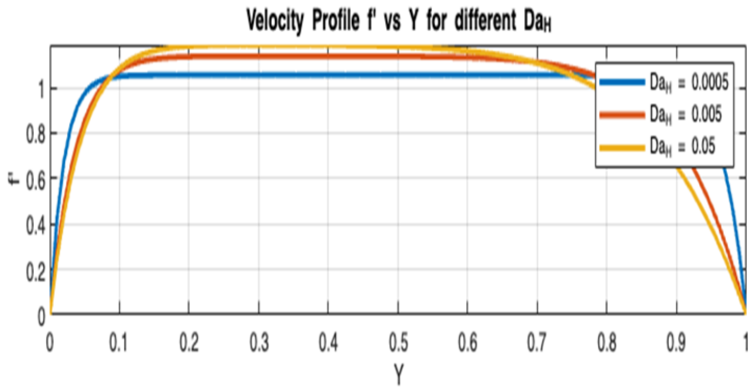

Figure 4 (b) variation of f' with respect to Da_H

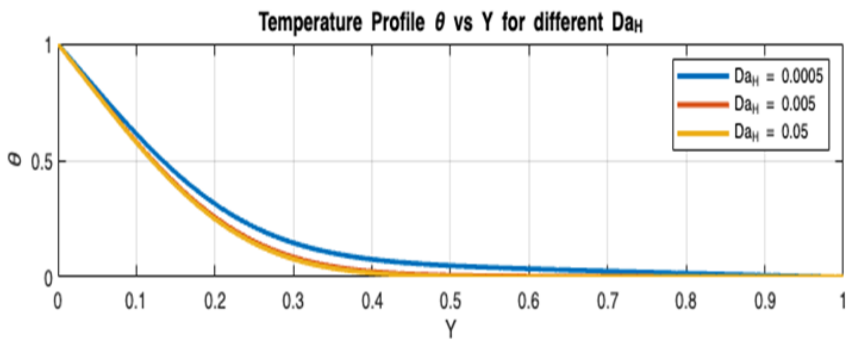

figure 4 (c) variation of θ with respect to Da_H

Study of the Reynolds number

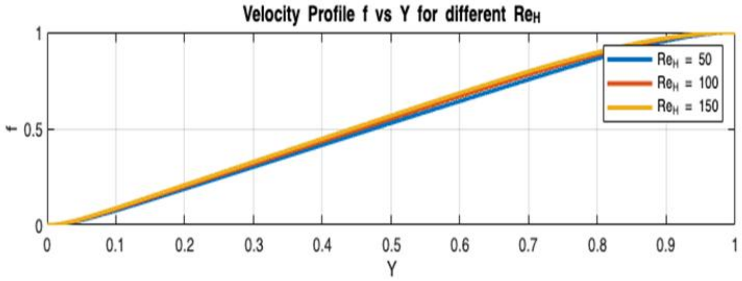

figure 5 (a) Variation of f with respect to Re_H

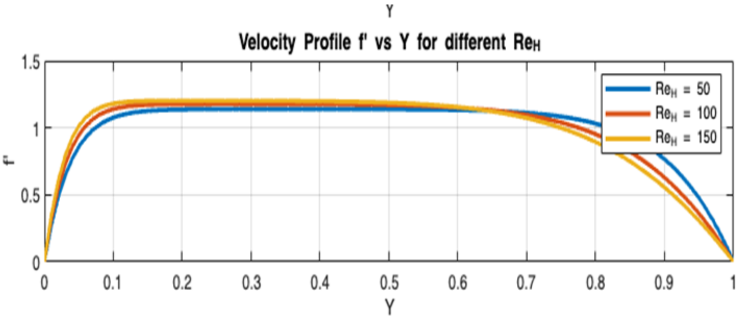

figure 5 (b) Variation of f' with respect to Re_H

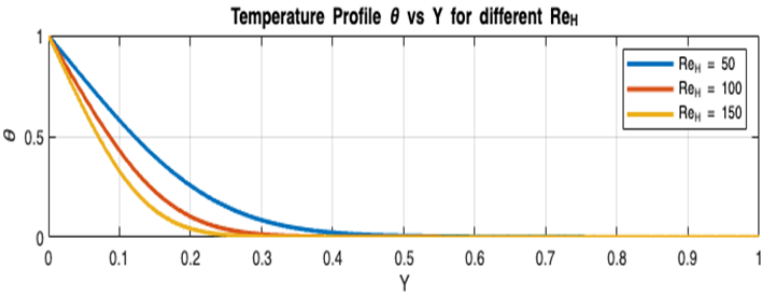

figure 5 (c) Variation of θ with respect to Re_H

Hartmann number study

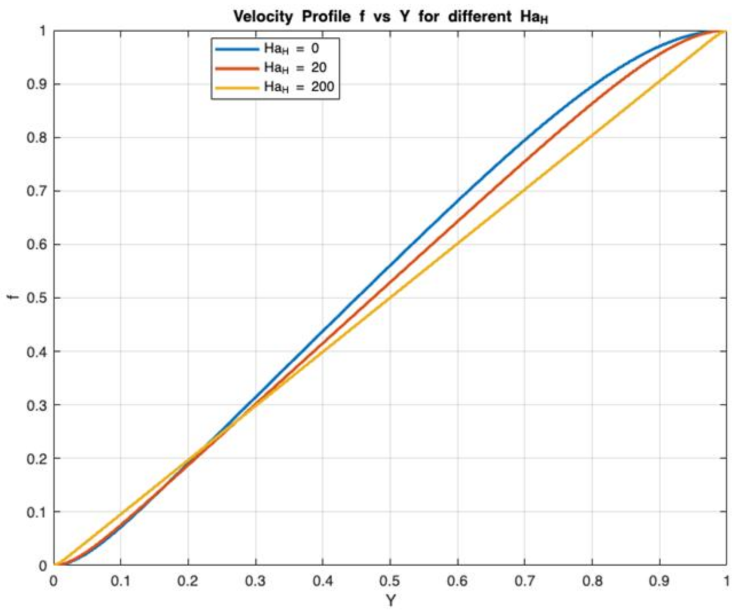

Figure 6 (a) Variation of distribution of f with respect to Ha_H

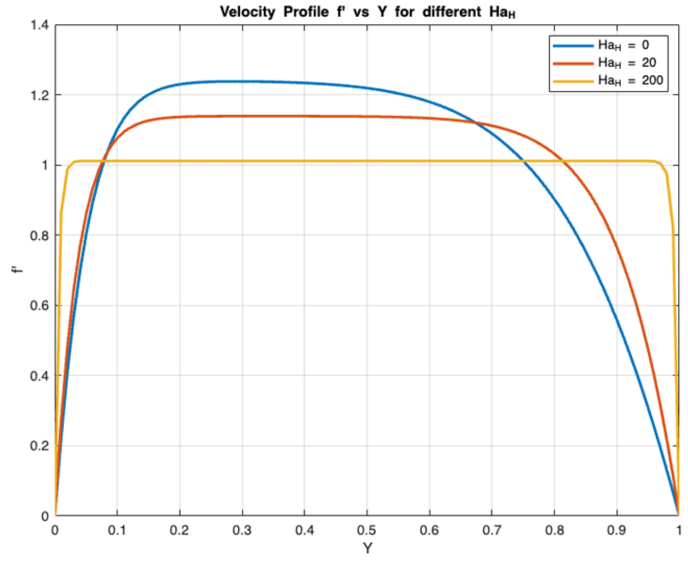

Figure 6 (b) Variation of distribution of f' with respect to Ha_H

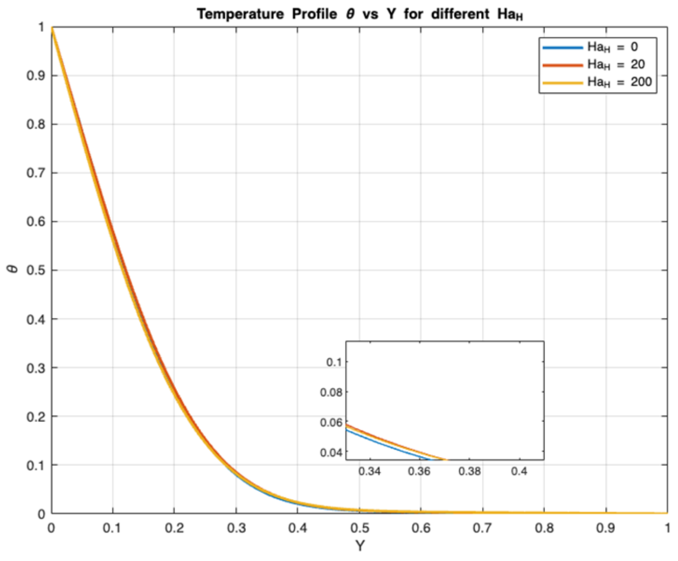

Figure 6 (c) 1 Variation of distribution of θ with respect to Ha_H

Investigating effect of Hartmann number on Nusselt at different porosity

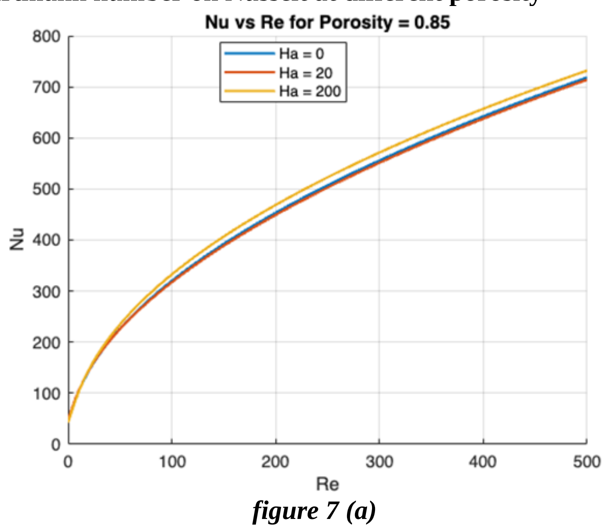

figure 7 (a)

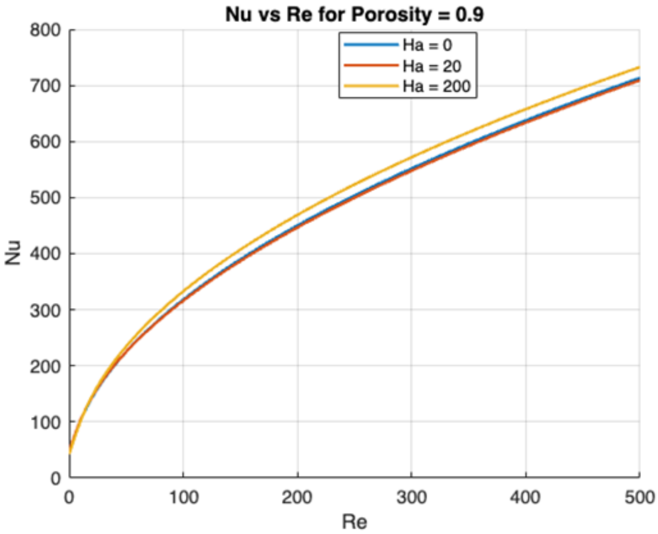

figure 7 (b)

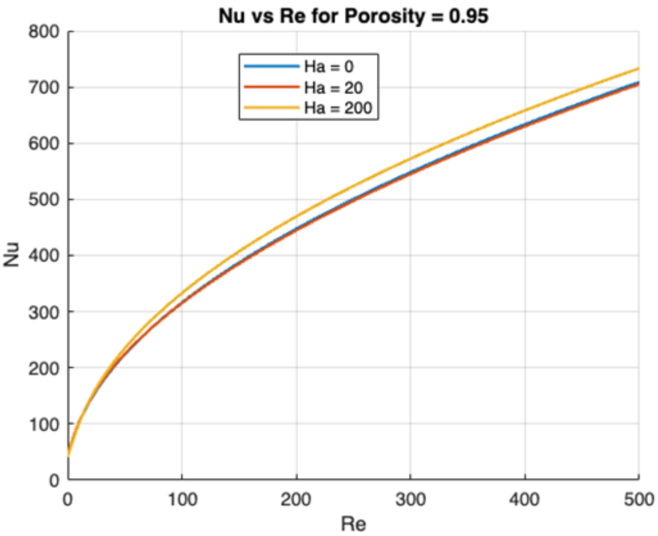

fugure 7 (c)

IV. Discussion

Based on the rule of mixtures, the base fluid has a density of 1.128 g/cm³, while the nanofluid's density is calculated to be 1.1616 g/cm³. This indicates that the addition of CNTs results in a slight increase in the density of the Polyethylene Glycol base fluid. The increase in density may have implications for various applications of CNT-based nanofluids, such as thermal management. Increased mixture density results in better thermal performance, enabling electronic devices to operate at lower temperatures. This is particularly crucial for high-power electronic components, where effective cooling is essential to maintain optimal performance and reliability.

The viscosity of the CNT-PEG-400 nanofluid increases compared to the viscosity of the base fluid due to the addition of CNTs. While the increase in viscosity of a CNT-based nanofluid in PEG-400 can enhance heat transfer performance, it also poses challenges such as higher energy consumption and pressure drop. Balancing these factors is critical in optimizing thermal management systems for efficient cooling while ensuring stability and reliability.

Figure 4 illustrates the changes in the distributions of (f), (f′), and (θ) in relation to (Da_H). According to Equation (8), (f) and (f′) represent the non-dimensional velocity components in the y-direction and x-direction, respectively. As illustrated in Figure 4(a), the function (f) exhibits an almost linear increase with (Y). This trend signifies a shift in velocity from a purely vertical flow to a point of zero velocity as the fluid ascends from the fan positioned above the porous medium to the heated surface. With an increase in (Da_H), (f) exhibits a slight rise. This is attributed to the enhanced permeability of the porous medium, which facilitates easier fluid flow along the fan's direction. As (Da_H) becomes larger, the y-component of the velocity vector increases, while the x-component decreases. The variation of (f′) in Fig. 4(b) also supports this observation. In Fig. 4(b), (f′)

exhibits a step increase with (Y) near the hot wall, indicating the boundary layer thickness where a sharp velocity gradient is present. Another steep gradient region is observed around (Y = 1), representing the upper part of the porous area where the flow is predominantly vertical, gradually transitioning as it approaches the heated surface.

As (Da_H) increases, the permeability of the porous medium improves, reducing flow resistance. This results in lower velocity gradients within the boundary layer, leading to a thicker boundary layer near the fan-driven flow's impingement, a trend visible in Fig. 4(b). Since the shear stress and frictional losses on the heated surface are influenced by the velocity gradient within the boundary layer, the shear stress decreases as (Da_H) increases. In Fig. 4(c), the variable (θ) decreases nearly exponentially with (Y), approaching zero. The region with a high gradient near the wall (Y = 0) represents the thermal boundary layer. As (Da_H) rises, the temperature gradient near the wall becomes steeper, leading to a reduction in the thermal boundary layer thickness. Based on Fick's law, the temperature gradient at the wall correlates with the heat flux. Consequently, higher heat transfer rates are expected with increasing (Da_H). This aligns with physical expectations, as a more permeable porous medium enhances (f′) near the wall, thereby boosting convective heat transfer.

Figure 5 illustrates how the distributions of f, f′, and θ vary with the Reynolds number (Re_H) of the base fluid . As Re_H rises, the momentum input of the fluid in the y-direction also increases, resulting in enhanced values of f. However, since the flow remains in the laminar, f does not exhibit significant sensitivity to changes in Re_H.

From Fig. 5(b), it is evident that increasing Re_H enhances the gradientof f′ close to the wall, whereas the slope diminishes at the upper part of the porous medium. As the fluid moves into the porous foam, it flows vertically at first, then transitions to horizontal flow due to the impingement on the surface. An increase in Re_H boosts the fluid's momentum, enabling it to maintain its initial flow state over a longer distance. Consequently, the slope of the velocity profile (f′) at the upper surface of the porous foam decreases with higher Re_H. In the laminar regime, an increase in Re_H results in a reduction of the boundary layer thickness. This causes a steeper gradient of f′ near the heated wall, leading to greater friction losses as Re_Hincreases.

Fig. 5(c) shows that increasing Re_H reduces the temperature distribution θ while increasing its gradient close to the heated wall. Same as the effect of the Darcy number Da_H, the rise in Re_H increases the heat transfer performance, contributing to higher thermal performance.

Figure 6 illustrates the variations in the distributions of f, f′, and θ with respect to Ha_H for the base fluid. According to Equation (6), increasing (Ha_H) for the base fluid enhances the magnetic body force, which operates in the x-direction and is directly proportional to the velocity (U). The magnetic force alters the direction of the impiging flow, changing it from vertical to horizontal. As seen in Fig. 6, as Ha_H increases, f decreases, and the f′ profile flattens. This suggests that as the vertical impingement flow enters the porous region, the magnetic force redirects it more horizontally. The stronger the magnetic field, the greater the rate of deflection, as evident from the behaviour in Fig. 6(b).

The horizontal magnetic force facilitates the transition of flow near the wall from a stationary state to the mainstream velocity. This action reduces the boundary layer thickness and increases the shear stress on the wall. Fig. 6(c) illustrates the effect of Ha_H on the temperature profile θ. It is evident that an increase in the Hartmann number (Ha_H) has a negligible effect on the temperature distribution, since the Hartmann number does not directly affect the energy equation (Equation 4).

Figure 7 illustrates how the Hartmann number (Ha_H) influences the Nusselt number (Nu) in relation to the Reynolds number across various porosities. It can be seen that as porosity rises, Nu diminishes. This reduction is due to the decline in effective thermal conductivity, which is influenced by the increase in Ha_H, as demonstrated in Equation (3.6.1). The thermal performance of the heat sink is affected by the magnetic field, and this effect changes depending on the porosity. For ϵ=0.85, an increase in Ha_H has almost no effect on Nu. However, for ϵ=0.95, increasing Ha_H results in a rise in Nu.

As explained in Section above, increasing Ha_H enhances convective flow over the heated surface. Based on Eq. (4), a reduction in porosity enhances the impact of viscous dissipation on overall heat transfer. Since viscous dissipation negatively impacts heat transfer, at lower porosities, the enhanced convection because of the the magnetic force is counteracted by dissipation, reducing the heat transfer rate. At higher porosities, the impact of viscous dissipation decreases, leading to improved heat transfer due to the increase in Hartmann number (Ha_H).

V. Conclusion

- CNTs increase the density and viscosity of PEG-400, contributing to better thermal performance.
- **Increasing Darcy number** enhances the profiles of the velocity and heat transfer, improving overall cooling performance.
- **Increasing the Hartmann number** reduces velocity profiles, leading to varying effects on heat transfer depending on porosity. For porosities beyond 0.9, a rise in Hartmann number results in an increase in Nusselt Number, thus, improving heat transfer performance.

These results contribute to optimizing cooling strategies for electronic devices, especially under the influence of magnetic fields, and highlight the significant role of porosity in determining the effectiveness of CNT-PEG-400 nanofluids in thermal management.

References

[1]. Ahmadi, G., Toghraie, D., Sedighi, K., & Karimipour, A. (2018). A Review On Nanofluids: Preparation, Stability Mechanisms, Thermal Conductivity, And Applications. Journal Of Molecular Liquids, 266, 420-437. Doi:10.1016/J.Molliq.2018.06.106
[2]. Calmidi, V. V., & Mahajan, R. L. (2000). Forced Convection In High Porosity Metal Foams. J. Heat Transfer, 122(3), 557-565.
[3]. Dhinesh Kumar, R., & Suresh, S. (2021). Magnetic Field-Induced Thermal Convection Of Nanofluids In Geothermal Applications. Geofluids, 2021, 3209855.
[4]. Do, K. H., Kim, T. H., & Kim, S. J. (2010). Analytical And Experimental Investigations On Fluid Flow And Thermal Characteristics Of A Plate-Fin Heat Sink Subject To A Uniformly Impinging Jet. International Journal Of Heat And Mass Transfer, 53(9-10), 2318-2323.
[5]. Einstein, A. (1926). A New Determination Of Molecular Dimensions. Annalen Der Physik, 324(2), 289-306.
[6]. Feng, S. S., Kuang, J. J., Lu, T. J., & Ichimiya, K. (2015). Heat Transfer And Pressure Drop Characteristics Of Finned Metal Foam Heat Sinks Under Uniform Impinging Flow. Journal Of Electronic Packaging, 137(2), 021014.
[7]. Jang, B. K., Sakka, Y., & Woo, S. K. (2009, March). Alignment Of Carbon Nanotubes By Magnetic Fields And Aqueous Dispersion. In Journal Of Physics: Conference Series (Vol. 156, No. 1, P. 012005). IOP Publishing.
[8]. Li, W., Hu, L., Jiang, C., & Li, W. (2020). Preparation, Characterization And Application Of Carbon Nanotube Based Nanofluids. Renewable And Sustainable Energy Reviews, 117, 109466.
[9]. Cwynar, K., Dziadosz, J., Scheller, Ł., Zorębski, E., Jędrysiak, R., Kolanowska, A., ... & Dzida, M. (2023). On Isobaric Heat Capacity Of Ionanofluids With Carbon Nanotubes–An Experimental Study. Journal Of Molecular Liquids, 387, 122535.
[10]. Li, X., Tu, Y., Zhao, Y., Hu, X., Liu, B., & Huang, Y. (2018). Synthesis Of Carbon Nanotubes By Catalytic Chemical Vapor Deposition Using A Single Precursor: Acetylene. Materials Research Express, 5(5), 055602.
[11]. Lou, D., Grablander, T., Mao, M., Hong, H., & Peterson, G. P. (2021). Improved Thermal Conductivity Of PEG-Based Fluids Using Hydrogen Bonding And Long Chain Of Nanoparticle. Journal Of Nanoparticle Research, 23, 1-10.
[12]. Mahian, O., Kolsi, L., Amani, M., Estellé, P., Ahmadi, G., Kleinstreuer, C., ... & Pop, I. (2019). Recent Advances In Modeling And Simulation Of Nanofluid Flows-Part I: Fundamentals And Theory. Physics Reports, 790, 1-48.
[13]. Marcos, M. A., Podolsky, N. E., Cabaleiro, D., Lugo, L., Zakharov, A. O., Postnov, V. N., ... & Semenov, K. N. (2019). MWCNT In PEG-400 Nanofluids For Thermal Applications: A Chemical, Physical And Thermal Approach. Journal Of Molecular Liquids, 294, 111616.
[14]. Narang, J. And Pundir, C.S. (2018) Current And Future Developments In Nanomaterials And Carbon Nanotubes. Volume 1, Introduction To Carbon Nanomaterials. Sharjah, UAE: Bentham Science Publishers.
[15]. Pourrahmani, H., Moghimi, M., Siavashi, M., & Shirbani, M. (2019). Sensitivity Analysis And Performance Evaluation Of The PEMFC Using Wave-Like Porous Ribs. Applied Thermal Engineering, 150, 433-444.
[16]. Sarkar, S. (2019). Nanofluids: Fundamentals, Properties And Applications. Wiley.
[17]. Shampine, L. F., Gladwell, I., & Thompson, S. (2003). Solving Odes With Matlab. Cambridge University Press.
[18]. Sigma-Aldrich. (N.D.). Polyethylene Glycol 400. Material Safety Data Sheet. Retrieved From Https://Www.Sigmaaldrich.Com
[19]. Sudhakar, N., & Ravi Kumar, P. V. (2014). The Behavior Of Nano-Fluids Under The Influence Of Magnetic Field. International Journal Of Advanced Research In Electrical, Electronics And Instrumentation Engineering, 3(3), 10783-10793.
[20]. Uglea, C. V. (1998). Oligomer Technology And Applications. CRC Press.
[21]. Wang, B., Zhang, Y., Li, X., Liu, H., & Zhao, J. (2019). Experimental Study On Heat Transfer Characteristics Of Carbon Nanotube Nanofluids Under A Magnetic Field. Applied Sciences, 9(7), 1409.
[22]. Whelan, B. P., Kempers, R., & Robinson, A. J. (2012). A Liquid-Based System For CPU Cooling Implementing A Jet Array Impingement Waterblock And A Tube Array Remote Heat Exchanger. Applied Thermal Engineering, 39, 86-94.
[23]. Xie, H., Chen, L., Wang, J., Shen, X., & Yang, Y. (2018). Experimental Study On The Viscosity Of Carbon Nanotube Aqueous Nanofluids Under Magnetic Field. Nanomaterials, 8(6), 393.
[24]. Yadav, D., Nirala, A., Kumar, R., & Singh, P. K. (2021). Density Variation In Nanofluids As A Function Of Concentration And Temperature. Materials Today: Proceedings, 46, 6576-6580.
[25]. Yin, Q., Sun, K. N., Li, A. J., Shao, L., Liu, S. M., & Sun, C. (2008). Study On Carbon Nanotube Reinforced Phenol Formaldehyde Resin/Graphite Composite For Bipolar Plate. Journal Of Power Sources, 175(2), 861-865.
[26]. Younes, H., Christensen, G., Li, D., Hong, H., & Ghaferi, A. A. (2015). Thermal Conductivity Of Nanofluids. Journal Of Nanofluids, 4(2), 107-132.
[27]. Younes, H., Mao, M., Murshed, S. S., Lou, D., Hong, H., & Peterson, G. P. (2022). Nanofluids: Key Parameters To Enhance Thermal Conductivity And Its Applications. Applied Thermal Engineering, 207, 118202.
[28]. Yu, W., Liu, C. & Fan, S. Advances Of CNT-Based Systems In Thermal Management. Nano Res. 14, 2471–2490 (2021). Https://Doi.Org/10.1007/S12274-020-3255-1
[29]. Zing, C., Mahjoob, S., & Vafai, K. (2019). Analysis Of Porous Filled Heat Exchangers For Electronic Cooling. International Journal Of Heat And Mass Transfer, 133, 268-276.